Composite-bonded Steel Substrate with Silyl-modified Polymer Exposed to Thermal Distress

Yail J. Kim[a*], Seung Won Hyun[b], Isamu Yoshitake[c], Jae-Yoon Kang[d], and Junwon Seo[e]
[a]University of Colorado Denver, Denver, CO, USA
[b]North Dakota State University, Fargo, ND, USA
[c]Yamaguchi University, Ube, Japan
[d]Korea Institute of Construction Technology, Ilsan, Korea
[e]South Dakota State University, Brookings, SD, USA

Abstract: This paper discusses a research program examining the residual performance of carbon fiber reinforced polymer (CFRP)-steel interface bonded with an emerging adhesive called silyl-modified polymer (SMP) when exposed to elevated temperatures from 25°C to 200°C. Double-lap tension specimens are prepared and conditioned at predefined temperatures for three hours. Test results reveal that interfacial capacity is preserved up to a temperature of 100°C. Thermally-induced capacity degradation is, however, observed for the specimens exposed to temperatures beyond 100°C. A phase-transition is noticed in adhesive morphology during heating at temperatures higher than 175°C, which affects the adhesion properties of the SMP. The development of CFRP strain is influenced by geometric discontinuities along the interface. Fiber disintegration dominates the failure of the interface exposed up to 150°C, including local fiber dislocation and partial CFRP pull-out. CFRP-debonding is, however, the primary failure mode for the specimens exposed to a temperature higher than 175°C. The Bayesian updating method is used to probabilistically infer the response of the CFRP-steel interface.

Keywords: carbon fiber reinforced polymer (CFRP); interface; silyl-modified polymer (SMP); temperature

1. INTRODUCTION

Structural strengthening is frequently implemented with carbon fiber reinforced polymer (CFRP) composites with polymeric adhesives. Some notable benefits of such an adhesive are resistance to chemicals, favorable density, formability, and toughness [1]. Of many types of bonding agents, an epoxy is broadly used for strengthening steel members with CFRP sheets [2]. Premature CFRP-debonding may be associated when excessive interfacial stress is applied. Previous studies report that stress localizations near geometric discontinuities such as CFRP termination trigger CFRP-debonding and stiff epoxy adhesives may not fully absorb applied interfacial stress [3]. To enhance the behavior of CFRP-steel interface (i.e., stress dissipation), an alternative bonding agent may be necessary. Silyl-modified polymer (SMP) is a newly developed material having strong elastic properties, including significant resistance to damping and cyclic load [4]. The potential application of SMP has recently been reported. Di Bella et al. [4] conducted a single-lap joint test with an SMP adhesive. Three-dimensional tomography was done to examine the failure modes of the specimens. Cohesion failure was a dominant failure mode. Kim et al. [3] suggested a hybrid bond configuration for CFRP-steel interface using an epoxy and an SMP to achieve load-bearing capacity with reduced interfacial stresses. Predicted models were proposed to assess the degree of stress alleviation in the interface.

Although the bond performance of aforementioned polymeric adhesives is satisfactory, thermally-induced distress is a critical consideration. A transition of mechanical properties is observed for a thermosetting polymer subjected to high temperatures, in particular beyond its glass transition temperature [5]. Provided all structural members are potentially exposed to fire hazards, thermal

* jimmy.kim@ucdenver.edu

responses of polymer-based interface should thoroughly be elucidated. da Silva and Adams [6] tested joints having dissimilar adherends bonded with multiple epoxies when exposed to elevated temperatures varying from -55°C to 200°C. Test results showed the behavior of the joint bonded with dual adhesives was superior to that of a single adhesive. Banea et al. [7] studied the fracture properties of a high temperature epoxy based on the double cantilever beam method. Test specimens were exposed to elevated temperatures up to 200°C. Finite element modeling was conducted to predict the specimen behavior. It was found that fracture toughness of the epoxy was not affected by temperatures below its glass transition temperature. Moussa et al. [8] evaluated the residual behavior of an epoxy exposed to 150°C for 4 hours. Test specimens were prepared as per ASTM-D638 (*Standard test method for tensile properties of plastics* [9]) and monotonically tested after thermal exposure was completed. Although the applied temperature was higher than the material's glass transition temperature, the properties of the adhesive did not significantly change. A post-curing effect was observed, which enhanced mechanical responses of the adhesive. To the best knowledge of the authors, there has been no research on the thermal response of SMP-bonded interface.

This paper presents a research program as to the temperature-dependent performance of CFRP-steel interface bonded with an SMP adhesive when exposed to elevated temperatures ranging from 25°C to 200°C. Emphasis was placed on thermal stress effects and failure characteristics. A probability-based model (i.e., Bayesian updating) was developed to predict the behavior of the interface.

2. RESEARCH SIGNIFICANCE

SMP may address the fundamental concern of the CFRP-steel interface (i.e., premature debonding when bonded with an epoxy adhesive) because it can effectively mitigate stress localization along the interface. The behavior of SMP-bonded interface is not well understood when thermal distress is applied. The test program conducted examines the residual behavior of the CFRP-steel interface bonded with SMP after exposing to high temperature. Technical results include load-carrying capacity, strain profile, and failure modes. Interfacial fracture energy is estimated using probability theory.

3. EXPERIMENTAL PROGRAM

A test program was carried out to examine the residual performance of the CFRP-steel interface bonded with an SMP adhesive when exposed to elevated temperatures. A summary of the experiment is provided in this section.

3.1. Materials

The SMP included a tensile strength of 2.6 MPa with an elastic modulus of 3.6 MPa and an elongation capacity of 250% [10]. This material is solvent-free and demonstrates significant elastic characteristics up to a temperature of 100°C. The volume change ratio of the SMP is less than 3% according to DIN52451 [11], which indicates favorable geometric stability after curing. The manufacturer suggests a thickness of 2 mm in practice. The steel strips used had a thickness of 3 mm and were mild steel with a specific yield strength of 413 MPa and corresponding modulus of 200 GPa. CFRP sheet (t = 0.165 mm) included a nominal tensile strength of 3800 MPa with a modulus of 227 GPa [12].

3.2. Details of Specimens

The temperature-dependent behavior of the CFRP-steel interface bonded with SMP was examined using double-lap specimens, as shown in Fig. 1(a). The surface of the steel substrate was roughened using an electrical grinder to improve bond with the adhesive. A single layer of CFRP was bonded to both sides of the prepared steel substrate [Fig. 1(a)]. All test specimens were cured for two weeks at

(a) (b) (c)

Figure 1: Test details: (a) double-lap specimen; (b) thermal exposure; (c) mechanical testing

room temperature before exposing to elevated temperatures. Thermal exposure was achieved within a range from 25°C to 200°C at an interval of 25°C for three hours. Such a testing plan can be justified by the fact that most structural members are subjected to a temperature up to 200°C for the first three hours when a fire takes place because they are insulated [13]. Table 1 summarizes the details of the test specimens: five specimens were repeatedly tested to address the stochastic nature of bond deterioration. The ID of the double-lap (DL) specimens used in Table 1 shows an exposure temperature and the number of repetition.

3.3. Experimental Plan and Instrumentation

The cured double-lap specimens were submitted to thermal exposure in an electric furnace. All specimens in a temperature category were heated simultaneously, as shown in Fig. 1(b). When the planned three hour of thermal exposure was completed, the specimens cooled down to room temperature. To measure the interfacial behavior of the conditioned specimens, strain gages were bonded along the CFRP [Fig. 1(a)]. Each specimen was then mechanically tensioned at a rate of 0.5 mm/min until failure occurred [Fig. 1(c)]. A data acquisition system was used to record the applied load, displacement, and strain.

4. EXPERIMENTAL RESULTS

4.1. Capacity of CFRP-steel Interface

The temperature-dependent residual capacity of each specimen is summarized in Table 1. Some scatter was noticed because the specimens were made by the wet-lay-up method. An average ultimate capacity of 3.6 kN was obtained for the control specimens (the DL25 series) with a standard deviation of 0.39 kN. The capacity of the test specimens was reasonably preserved up to an exposure temperature of 100°C (Table 1), while the capacity in this temperature range tended to increase. Such an observation may be attributable to a secondary curing (or bond-hardening) process that would condense the polymeric chains of the SMP adhesive [14]. The specimens exposed to temperatures higher than 100°C exhibited thermal damage. For instance, the interfacial capacity of the specimens subjected to 125°C and 150°C was 9.3% lower, on average, than that of the specimens exposed to 25°C to 100°C. The specimens at 175°C and 200°C demonstrated significantly low capacity (i.e., 0.38 kN on average). This illustrates that the SMP adhesive almost lost its adhesion capability beyond a temperature of 175°C, possibly due to the scission of its polymeric crosslink [15]. It is worthwhile to note that carbon fibers are not susceptible to temperature up to at least 1000°C [16]. According to observations in the laboratory, the specimens exposed to a temperature higher than 175°C revealed an obvious phase transition from crystalline-solid to amorphous-solid. In other words, thermal decomposition caused bond-weakening that changed the state of the SMP adhesive from completely

Table 1: Test details

Specimen	Temperature	Failure load (kN)	Fracture energy (N/mm)
DL25-1	25°C	3.15	1.13
DL25-2	25°C	3.43	0.77
DL25-3	25°C	3.55	0.85
DL25-4	25°C	4.22	0.61
DL25-5	25°C	3.65	0.62
DL50-1	50°C	3.92	0.77
DL50-2	50°C	4.08	0.70
DL50-3	50°C	4.01	0.83
DL50-4	50°C	3.58	0.55
DL50-5	50°C	3.62	0.62
DL75-1	75°C	3.66	0.51
DL75-2	75°C	3.93	0.84
DL75-3	75°C	3.81	0.79
DL75-4	75°C	3.49	0.40
DL75-5	75°C	4.24	0.64
DL100-1	100°C	3.60	0.69
DL100-2	100°C	3.59	0.62
DL100-3	100°C	3.96	0.64
DL100-4	100°C	3.78	0.52
DL100-5	100°C	4.56	0.84
DL125-1	125°C	3.19	0.73
DL125-2	125°C	2.71	0.86
DL125-3	125°C	3.67	0.93
DL125-4	125°C	3.74	0.43
DL125-5	125°C	3.91	0.61
DL150-1	150°C	3.74	0.97
DL150-2	150°C	3.20	0.60
DL150-3	150°C	3.09	0.80
DL150-4	150°C	3.60	0.44
DL150-5	150°C	3.56	0.50
DL175-1	175°C	0.23	0.01
DL175-2	175°C	0.41	0.03
DL175-3	175°C	0.38	0.03
DL175-4	175°C	0.53	0.03
DL175-5	175°C	0.35	0.03
DL200-1	200°C	0.21	0.01
DL200-2	200°C	0.19	0.01
DL200-3	200°C	Premature failure	Premature failure
DL200-4	200°C	Premature failure	Premature failure
DL200-5	200°C	Premature failure	Premature failure

hardened resin to rubber-like mushy resin. Upon cooling down to room temperature, the SMP state was reversed from amorphous-solid to crystalline-solid.

4.2. Load-displacement

The load-displacement response of selected specimens is provided in Fig. 2. For the specimens exposed a temperature up to 150°C, the load increased in a linear manner until a peak was achieved and then suddenly decreased. However, those subjected to a temperature of 175°C and above did not illustrate such a clear trend in load-displacement behavior because of the significant thermal damage accumulated during the heat exposure process. The residual stiffness of the double-lap specimens is shown in Fig. 3, which was obtained in a load range between 0% and 60% of the ultimate load (P_u) of

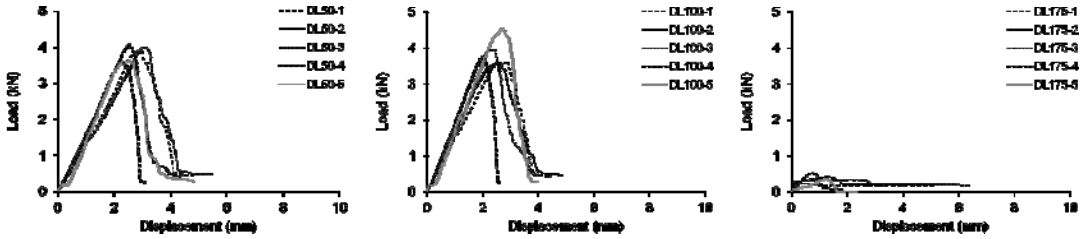

(a) (b) (c)

Figure 2: Load-displacement response: (a) exposed at 50°C; (b) exposed at 100°C; (c) exposed at 175°C

each specimen. A propensity for increasing stiffness was found in the specimens subjected to temperatures up to 100°C, while the stiffness gradually decreased beyond a temperature of 125°C.

4.3. Fracture Energy

Table 1 summarizes the interfacial fracture energy (G_f) of all the specimens, which was calculated using:

$$G_f = \frac{P_{\max}\delta_{\max}}{2n(L_{bond}b_{bond})} \tag{1}$$

where P_{max} and δ_{max} are the maximum load of the specimen and corresponding displacement; n is the number of bonded surface; and L_{bond} and b_{bond} are the CFRP bond length and width, respectively. The fracture energy was assumed to be evenly distributed along the interface between the CFRP and steel substrate. This assumption cannot reflect a nonlinear shear stress distribution; however, it is commonly accepted in engineering fracture mechanics. With an increasing temperature from 25°C to 75°C, the fracture energy decreased from 0.80 N/mm to 0.63 N/mm, on average. The energy became stable within a temperature range from 100°C to 150°C, and then dramatically decreased beyond 175°C.

4.4. Interfacial Strain

Figure 4 presents the development of interfacial strain. The strains near the geometric discontinuity (Gages 2 and 3) of the control specimen in Fig. 4(a)(i.e., middle of the specimen where the two strips contact) rapidly developed than those far from the discontinuity (Gages 1 and 4). This observation implies that a shear-lag has occurred along the interface, which delayed strain propagation. An elastic recovery was noticed when the specimen failed, evidenced by the unloading strain path. The specimen exposed to 150°C [Fig. 4(b)] demonstrated similar behavior to that of 25°C, while the deformation of

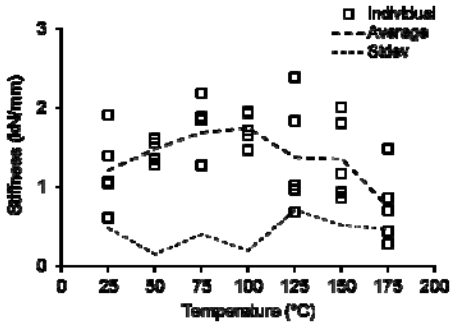

Figure 3: Residual stiffness of double-lap specimens

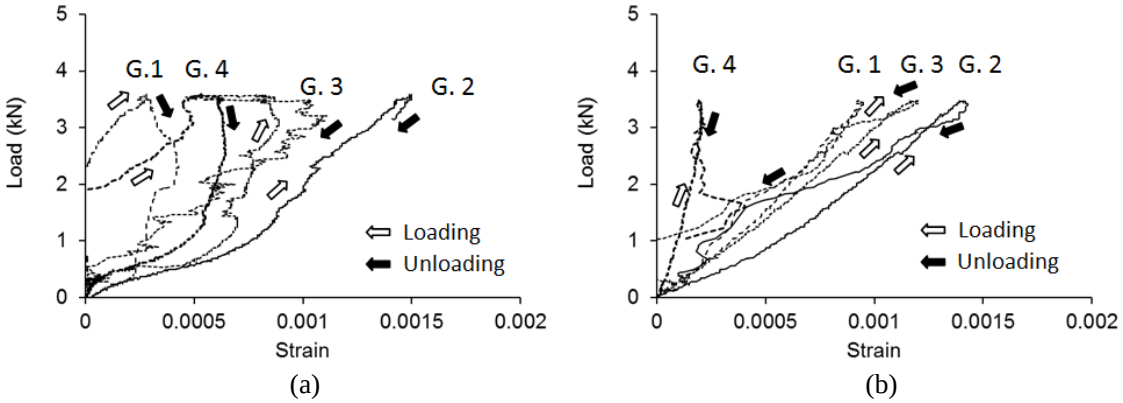

Figure 4: Load-strain behavior: (a) exposed at 25°C; (b) exposed at 150°C

the SMP layer was somewhat larger. It is, therefore, concluded that the presence of a geometric discontinuity was a contributing factor to increasing strain localization regardless of thermal exposure.

4.5. Failure Characteristic

Figure 5 shows the failure mode of the test specimens. For the case of the specimens exposed to 100°C, fiber disintegration was the primary failure mode [Fig. 5(a)]. This kind of failure was commonly observed for the specimens subjected to a temperature up to 150°C. Figure 5(b) further details the fiber disintegration with complex local fiber dislocation and CFRP pull-out. The specimen groups subjected to a temperature over 175°C exhibited CFRP-debonding without fiber disintegration [Fig. 5(c)]. It implies that the adhesion capability of the adhesive was significantly degraded due to the thermal exposure and hence adhesion failure controlled the failure of the double-lap specimens.

5. PRIDICTIVE MODELING

A probability-based theoretical model was developed to understand the thermal response of the CFRP-steel interface, based on the Bayesian updating method. The model was expected to expand the experimental investigation with limited test data. A summary of the predictive approach is provided in this section.

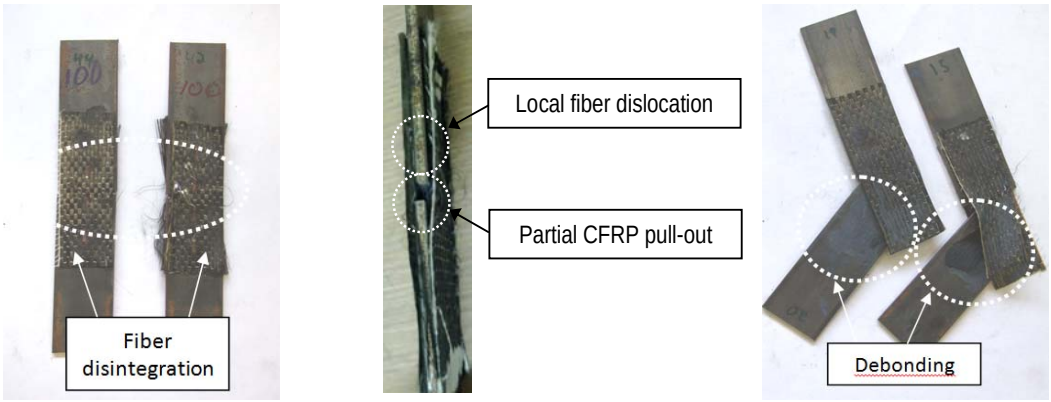

Figure 5: Failure mode: (a) exposed at 100°C; (b) typical fiber disintegration; (c) exposed at 175°C

5.1. Normality Test

The Anderson Darling method (Eq. 2 to 4 [17]) was used to test the normality of the interfacial fracture energy measured in the laboratory with the following hypothesis:

- H_o: the experimental fracture energy follows a normal probability distribution
- H_a: the experimental fracture energy does not follow a normal probability distribution

$$G_{f-std}(T) = \frac{G_{fi}(T) - G_{fms}(T)}{\sqrt{\frac{1}{n-1}\sum_{i=1}^{n}\left(G_{fi}(T) - G_{fms}(T)\right)^2}} \text{ and } G_{fms}(T) = \frac{\sum_{i=1}^{n} G_{fi}(T)}{n} \quad (2)$$

$$A^2 = -n - S \quad (3)$$

$$S = \sum_{i=1}^{n} \frac{(2i-1)}{n}\left[\ln\left(F\left(G_{f-std}(T)\right)\right) + \ln\left(1 - F\left(G_{f-std(n+1-i)}\right)\right)\right] \quad (4)$$

where $G_{f\text{-}std}(T)$ is the standardized fracture energy at a temperature T; n is the number of samples; $G_{fi}(T)$ and $G_{fms}(T)$ are the i^{th} fracture energy and corresponding mean energy of the samples taken from the test, respectively; and F is the standard normal cumulative distribution function. The distribution of the interfacial fracture energy was found to be normal (Table 2), given the aforementioned hypothesis H_0 was not rejected because the p value of Eq. 3 for all the test specimens was greater than a level of significance $\alpha = 0.05$.

Table 2: Normality Test

Temperature	*p* value	Temperature	*p* value
25°C	0.361	125°C	0.825
50°C	0.892	150°C	0.575
75°C	0.715	175°C	0.101
100°C	0.603	200°C	0.227

5.2. Prior Distribution and Data Sampling

The means and standard deviations of temperature-dependent fracture energy were obtained from the test data shown in Table 1. The number of randomly sampled data was 1000 per temperature. Figure 6(a) shows an example for data sampling at 25°C with $N(0.80, 0.21^2)$ and Fig. 6(b) reveals a convergence study supporting the adequacy of the sample size selected. The posterior distribution of the mean and standard deviation of the fracture energy was inferred based on the concept of a non-informative prior distribution (i.e., uniform distributions were initially assumed for the mean and the standard deviation).

5.3. Posterior Distribution of Mean Fracture Energy

Equation 5 represents a joint posterior distribution for the mean and variance of the interfacial fracture energy (G_{fm} and σ^2, respectively) at a temperature T:

$$P\left(G_{fm}, \sigma^2 \mid G_{f1,} G_{f2}, \ldots G_{fn}\right) \propto P\left(G_{f1,} G_{f2}, \ldots G_{fn} \mid G_{fm}, \sigma^2\right) P\left(G_{fm}, \sigma^2\right) \quad (5)$$

Equations 6 to 8 are derived from Eq. 5:

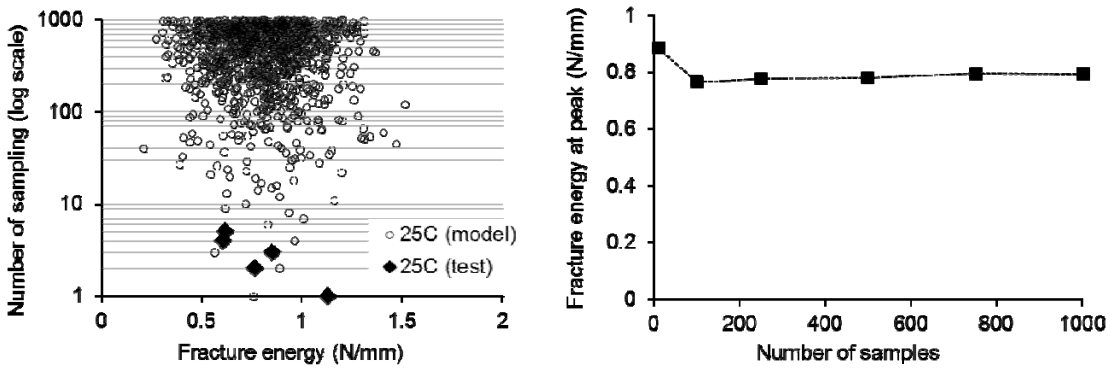

(a) (b)

Figure 6: Data sampling for Bayesian updating: (a) random sampling; (b) convergence study

$$\left(\sigma^2\right)^{-1}\left(\sigma^2\right)^{-\frac{n}{2}} Exp\left[-\frac{1}{2\sigma^2}\sum_{i=1}^{n}\left(G_{fi}-G_{fm}\right)^2\right] \tag{6}$$

or

$$\left(\sigma^2\right)^{-\frac{n+2}{2}} Exp\left[-\frac{1}{2\sigma^2}\left[(n-1)s^2+n\left(G_{fms}-G_{fm}\right)^2\right]\right] \tag{7}$$

$$s^2=\frac{1}{n-1}\sum_{i=1}^{n}\left(G_{fi}-G_{fms}\right)^2 \tag{8}$$

The posterior distribution of the mean fracture energy was calculated from Eqs. 6 to 8 with possible standard deviations (Eq. 9: marginal posterior distribution):

$$P\left(G_{fm}\mid G_{f1,}G_{f2},...G_{fn}\right)=\int_0^{\infty}\left(\sigma^2\right)^{-\frac{n+2}{2}} Exp\left\{-\frac{1}{2\sigma^2}\left[(n-1)s^2+n\left(G_{fm}-G_{fms}\right)^2\right]\right\}d\sigma^2 \tag{9}$$

The posterior distribution of G_{fm} is then obtained by

$$\frac{G_{fms}-G_{fm}}{s/\sqrt{n}}\approx t_{n-1} \tag{10}$$

Table 3 lists the updated G_{fm} using Eq. 10 at a 95% Bayesian confidence interval. The posterior distribution of the standard deviation can be obtained in a similar manner described in this subsection.

5.4. Predicted Posterior Distribution of Fracture Energy

The posterior distribution of individual interfacial fracture energy ($\tilde{G_f}$) may be predicted using:

Table 3: Mean and Standard Deviation for Fracture Energy- 95% Bayesian Confidence Interval

Temperature	Credible interval		Temperature	Credible interval	
	Mean	Stdev		Mean	Stdev
25°C	[0.792,0.819]	[0.204,0.223]	125°C	[0.689,0.715]	[0.187,0.205]
50°C	[0.683,0.696]	[0.104,0.113]	150°C	[0.656,0.682]	[0.211,0.231]
75°C	[0.627,0.651]	[0.176,0.192]	175°C	[0.024,0.025]	[0.011,0.012]
100°C	[0.655,0.670]	[0.114,0.124]	200°C	[0.0050,0.0051]	[0.00062,0.00067]

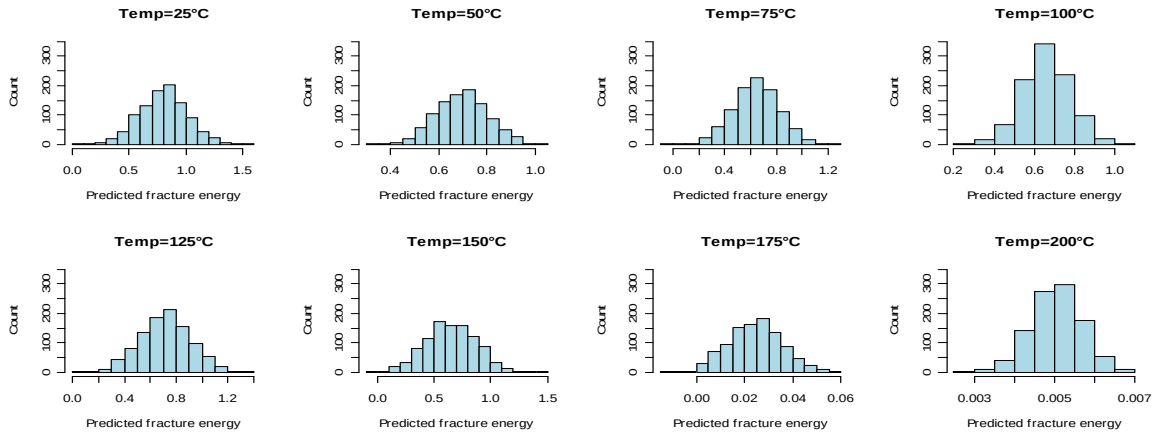

Figure 7: Population-level predicted distribution of interfacial fracture energy

$$P\left(\tilde{G}_f \mid G_{f1,}G_{f2},...G_{fn}\right)=\int_0^{\infty}\int_{-\infty}^{\infty}P\left(\tilde{G}_f \mid G_{f1,}G_{f2},...G_{fn},G_{fm},\sigma^2\right)P\left(G_{fm},\sigma^2 \mid G_{f1,}G_{f2},...G_{fn}\right)dG_{fm}d\sigma \tag{11}$$

It should be noted that Eq. 11 provides a population-level interfacial fracture energy for a specific temperature, while Eq. 9 indicates the inferred pattern of the mean fracture energy. The predicted posterior distribution of $\tilde{G}_f$ may be expressed as:

$$\frac{G_{fms}-\tilde{G}_f}{s\sqrt{1+1/n}} \approx t_{n-1} \tag{12}$$

Figure 7 exhibits the predicted posterior distribution of temperature-dependent fracture energy. A comparison between the test and the predictive method is made in Fig. 8. The mean fracture energy estimated by Eq. 9 was positioned at almost mid-range of the test data. The predictive envelops (Eq. 11) effectively covered the scatter of the experimental fracture energy. For design and practice, the proposed methodology can be used to probabilistically estimate the fracture energy of the CFRP-steel interface bonded with SMP subjected to elevated temperatures.

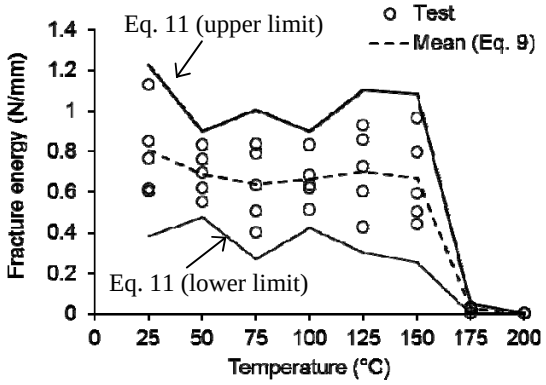

Figure 8: Comparison between test and prediction

6. CONCLUSIONS

This paper has discussed the residual performance of the CFRP-steel interface bonded with SMP subjected to elevated temperatures ranging from 25°C to 200°C. The experimental program provided interfacial capacity, CFRP strain, and failure characteristics, while the predictive model inferred the *true* fracture energy of the interface at a population level. The following is concluded:

- The interfacial capacity of the test specimens was maintained until 100°C, whereas noticeable thermal hysteresis was observed beyond 100°C. The adhesion capability of the adhesive was significantly reduced beyond a temperature of 175°C at which a morphological transition was observed in the furnace.
- The strain development of the interface was influenced by the geometric discontinuity at the gap between the two steel strips. A shear-lag mechanism was also noticed due to the delayed deformation of the SMP layer.
- Fiber disintegration was the primary source of the interfacial failure for the specimens exposed to temperatures up to 175°C, including local fiber dislocation and CFRP pull-out. The specimens subjected to a temperature higher than 175°C, however, revealed CFRP-debonding.
- The probability distribution of the interfacial fracture energy was found to be normal as per the Anderson Darling test. The *true* statistical properties were inferred by the Bayesian updating technique. The predicted fracture energy enveloped the upper and lower limits of the experimental fracture energy.

Acknowledgements

The authors wish to acknowledge financial support from the United States Department of Transportation through the Mountain-Plains Consortium Program. Undergraduate students, J. Gerber and T. Siriwardanage, have conducted the experimental work reported. The SMP material has been donated by Bostik, Inc.

References

[1] Baldan, A. "*Adhesively-bonded joints and repairs in metallic alloys, polymers and composite materials: adhesives, adhesion theories and surface pretreatment*", Journal of Materials Science, 39(1), 1-49, (2004).

[2] Zhao, X.-L. and Zhang, L. "*State-of-the-art review on FRP strengthened steel structures*", Engineering Structures, 29(8), 1808-1823, (2007).

[3] Kim, Y.J., LaBere, J., and Yoshitake, I. "*Hybrid epoxy-silyl modified polymer adhesives for CFRP sheets bonded to a steel substrate*", Composites Part B, 51, 233-245, (2013).

[4] Di Bella, G., Galtieri, G., Pollicino, E., and Borsellino, C. "*Mechanical characterization of adhesive joints with dissimilar substrates for marine applications*", International Journal of Adhesion and Adhesives, 41, 33-40, (2013).

[5] Lapique, F and Redford, K. "*Curing effects on viscosity and mechanical properties of a commercial epoxy resin adhesive*", International Journal of Adhesion and Adhesives, 22(4), 337-346, (2002).

[6] da Silva, L.F.M. and Adams, R.D. "*Adhesive joints at high and low temperatures using similar and dissimilar adherends and dual adhesives*", International Journal of Adhesion and Adhesives, 27(3), 216-226, (2007).

[7] Banea, M.D., da Silva, L.F.M., and Campilho, R.D.S.G. "*Mode I fracture toughness of adhesively bonded joints as a function of temperature: experimental and numerical study*", International Journal of Adhesion and Adhesives, 31(5), 273-279, (2011).

[8] Moussa, O., Vassilopoulos, A.P., de Castro, J., and Keller, T. "*Time-temperature dependence of thermomechanical recovery of cold-curing structural adhesives*", International Journal of Adhesion and Adhesives, 35, 94-101, (2012).

[9] ASTM. "*Standard test method for tensile properties of plastics (ASTM D-638-10)*", American Society for Testing and Materials, West Conshohocken, PA, USA, (2010).

[10] Bostik. "*Bostik 70-03A data sheet*", Bostik, Inc., Middleton, MA, USA, (2011).

[11] ANSI. "*Testing of sealing materials for buildings- part 1: determination of change in mass and volume of self-leveling joint sealants (DIN 52451)*", American National Standards Institute, Washington, D.C., USA, (2007).

[12] BASF. "*MBrace CF130 unidirectional high strength carbon fiber fabric for the MBrace composite strengthening system*", BASF Construction Chemicals, Shakopee, MN, USA, (2007).

[13] Kodur, V. K. R., Bisby, L. A., and Green, M. F. "*Guidance for the design of FRP-strengthened concrete members exposed to fire*", Journal of Fire Protection Engineering, 17(5), 5-26, (2007).

[14] Ehrenstein, G.W. "*Polymeric materials, Hanser Gardner Publications*", Cincinnati, OH, USA, (2001).

[15] Kholodovych, V. and Welsh, W.J. "*Thermal-oxidative stability and degradation of polymers*", Physical Properties of Polymers Handbook, 2nd edition, Springer, 927-938, (2007).

[16] Rostasy, F. "*Fiver composite elements and techniques as non-metallic reinforcement of concrete*", Brite Project 4142/BREU-CT910515, Evaluation of Potential and Production Technologies of FRP, Technical Report Task 1, (1992).

[17] Stephens, M. A. "*EDF statistics for goodness of fit and some comparisons*", Journal of the American Statistical Association, 69(347), 730-737, (1974).